MADRID
inter.noise 2019
June 16 - 19
NOISE CONTROL FOR A BETTER ENVIRONMENT

# Enhancement of acoustic black hole effect in beams using shunted piezo-electric patch

**Mi, Yongzhen[1]**
**State Key Laboratory of Mechanical System and Vibration, Institute of Vibration, Shock and Noise, Shanghai Jiao Tong University, Shanghai 200240, China**
**Room B402, ME School, Dongchuan Road 800, Shanghai, China**

**Zheng, Hui[2]**
**Collaborative Innovation Center for Advanced Ship and Deep-sea Exploration (CISSE), Shanghai 200240, China**
**Room A804, ME School, Dongchuan Road 800, Shanghai, China**

## ABSTRACT

**Acoustic black hole (ABH) effect is caused by embedding a power-law profiled taper into a host structure, which gradually reduces the bending wave velocity and thus facilitates vibration control. However, it is found that an imperfect taper with unavoidable truncation could significantly impair the ABH effect due to wave reflections at the truncated tip. This paper studies the use of shunted piezo-electric patch to mitigate this drawback and enhance the ABH effect in a Euler-Bernoulli beam. Firstly, an energy-based numerical model is built by decomposing the beam's flexural displacement to a set of admissible functions. Based on this model, the influences of shunting circuit's resistance on the ABH effect are studied in detail, and its energy dissipation is summarized to a three-phase transition characteristic. Finally, experiments are carried out to validate the numerical model's reliability, as well as to verify the enhancements brought about by the shunted piezoelectric patch.**

**Keywords:** Acoustic black hole, Piezoelectric patch, Resistive shunting circuit
**I-INCE Classification of Subject Number:** 47

## 1. INTRODUCTION

The conflicts between reducing a product's weight and suppressing its mechanical vibration has been a long-standing challenge to many industries. The practices for solving this dilemma promotes the emergence of Acoustic Black Hole (ABH). First proposed by Mironov [1] and further developed by Krylov [2], this concept introduces a taper with a power-law thickness profile into a beam or a plate, so that the local phase velocity of the bending wave could be gradually reduced while propagating towards the tip. Such property turns the ABH taper to an ideal anechoic termination, making it particularly appealing to vibration control and noise reduction applications. Many researchers have explored the dynamic characteristics of different structures embedded with various ABH designs, through both numerical studies [3, 4] and experimental investigations [5, 6].

A perfect power-law profile is impossible for current machining techniques to fabricate and there is always a small truncation at the thin edge with finite residual thickness. Despite being small, this truncation results in high reflection, making the ABH's ability to absorb elastic wave significantly impaired. It is found that coving the taper with thin damping layers could largely reduce the reflection, thanks to energy concentration in the ABH area that enables damping layers to work with much better efficiency. In general, damping treatments provides a reasonable way to compensate the truncation-induced loss of ABH effect, but their implementation is not without drawbacks. First, it counters to a lightweight product for which we in the first place start off. Also, the dissipative capacity of damping material is highly dependent on frequency and temperature, and in a real, uncertain world it may not act as effectively as what the theoretical studies assume it to be. Such weaknesses necessitate developments of alternative schemes to enhance the ABH effect.

In this paper, we propose to use the shunted piezoelectric patch as an alternative scheme to enhance the ABH effect. Instead of damping layers, the patch uses a purely resistive shunting circuit to damp down the elastic wave reflected by the truncation. In this paper, we investigate the influences of the resistance on the ABH effect and its energy dissipation characteristic, together with the influences of the piezo-patch's location, thickness and its mass-loading on the host beam. Finally, experiments are carried out to verify the reliability of the proposed characterization, as well as to affirm the enhancements brought about by the shunted piezoelectric patch.

## 2. Theoretical Model and Formulation

### 2.1 Model description

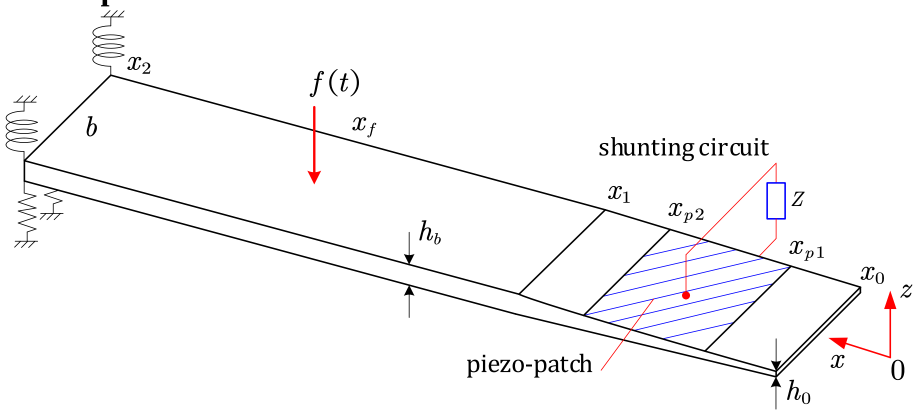


*Fig. 1. Illustration of an acoustic black hole beam consisting of a uniform slab and an acoustic black hole taper. The taper is covered by a piezo-electric patch linking to a shunting circuit.*

Fig. 1 illustrates an ABH beam with a rectangular cross-section, consisting of a uniform slab and the acoustic black hole taper. By placing the origin of coordinate system at the point where the thickness of the ABH taper eventually vanishes, the power-law profiled thickness can be expressed as $h(x) = \mu x^m$. The real taper, however, only spans $x_0$ to $x_1$, resulting in a truncated cross-section with thickness $h_0$. The uniform part between $x_1$ and $x_2$ has thickness $h_b$ and width $b$, on which a point force is applied at $x_f$. The ABH beam is assumed symmetrical to its mid-plane in the z-direction, with its taper end free and its uniform end elastically constrained by the transitional and rotational springs. Two piezo-electric patches are separately bonded to the upper and bottom surfaces of the taper, taking up the length between $x_{p1}$ and $x_{p2}$.

### 2.2 Governing equations

The material of the ABH beam is assumed to be isotropic and linearly elastic, characterized by its elastic modulus $E_b$, density $\rho_b$ and damping loss factor $\eta_b$. The equivalent elasticity modulus of the piezoelectric patch can be expressed as

$$E_p = \frac{h_p(1+iRC_p\omega)}{h_pS_{11}^E(1+iRC_p\omega)-iRd_{31}^2A_s\omega} \tag{1}$$

in which $i=\sqrt{-1}$ is the imaginary unit and $\omega$ is the angular frequency; $h_p$ and $A_s$ are the thickness and area of the electrodes; $C_p=\epsilon_{zz}^TA_s/h_p$ is the internal capacitance of the patch where $\epsilon_{zz}^T$ is the dielectric constant; $R$ is the prescribed resistance; $d_{31}$ is the electro-mechanical coupling constant.

Assuming the piezoelectric patch is firmly attached to the beam, the total elasticity modulus and total bending rigidity of the “patch-taper-patch” structure can be expressed as

$$E_t = \frac{2E_pA_p+\overline{E}_bA_b}{2A_p+A_b} \tag{2}$$

$$R_t = 2E_pI_p+\overline{E}_bI_b \tag{3}$$

in which $\overline{E}_b=E_b(1+i\eta_b)$ is the complex form the beam’s elasticity modulus.

The Lagrangian functional of the whole system is written as

$$L = E_k - E_p + W_f \tag{4}$$

where $E_k$ and $E_p$ are the kinematic energy and potential energy of the system, respectively; $W$ is the work done by external forces. Under the Euler-Bernoulli beam theory, the detailed expression of $E_k$ is written as

$$\begin{aligned} E_k = \frac{1}{2}\int_{x_1}^{x_2}\rho_bh_b\left(\frac{\partial w}{\partial t}\right)^2dx + \frac{1}{2}\int_{x_0}^{x_1}\rho_bh(x)\left(\frac{\partial w}{\partial t}\right)^2dx \\ + \frac{1}{2}\int_{x_{p1}}^{x_{p2}}\rho_ph_p\left(\frac{\partial w}{\partial t}\right)^2dx \end{aligned} \tag{5}$$

$E_p$ can be obtained by

$$\begin{aligned} E_p = \frac{1}{2}\int_{x_0}^{x_2}E_b\overline{I}_b(x)\left(\frac{\partial w}{\partial x}\right)^2dx + \frac{1}{2}\int_{x_{p1}}^{x_{p2}}2E_pI_p\left(\frac{\partial w}{\partial x}\right)^2dx \\ + \frac{1}{2}k_tw(x_2,t)^2 + \frac{1}{2}k_r\left(\frac{\partial w(x_2,t)}{\partial x}\right)^2 \end{aligned} \tag{6}$$

where $\overline{I}_b(x)=b\overline{h}^3(x)/12$ and $I_p=bh_p^2/12+bh_p(h_b/2+h_p/2)^2$ are the moments of inertia of the beam and the patch, respectively; $k_t$ and $k_r$ are stiffness of the transitional springs and the rotational springs, respectively.

Finally, $W_f$ is written as

$$W_f = f(t)w(x_f,t) \tag{7}$$

The flexural displacement $w$ of the beam is expressed as a linear combination of assumed admissible functions $\varphi(x)$

$$w(x,t) = \sum_i \lambda_i(t)\varphi_i(x) \tag{8}$$

Substituting Eqs. (5~8) into Eq. (4) and performing the first-order variational operation with regard to $\lambda_i(t)$, a series of linear equations are obtained and arranged into a matrix form

$$\mathbf{M}\ddot{\boldsymbol{\lambda}}(t) + \mathbf{K}\boldsymbol{\lambda}(t) = \mathbf{f}(t) \tag{9}$$

where $\mathbf{M}$ and $\mathbf{K}$ are the generalized mass matrix and generalized stiffness matrix, respectively; $\boldsymbol{\lambda}(t)$ and $\mathbf{f}(t)$ are vectors of generalized coordinates and external force.

## 3. Numerical Results and Discussion

### 3.1 System configuration

The boundary condition of the beam is set clamped-free, achieved by assigning $k_t$ and $k_r$ in Eq. (10) by $10^8 E_b I_b$. The geometrical parameters and material constants of the beam and the piezo-patch are shown in Table 1.

*Table 1 Geometrical parameters and material constants of the beam and the piezo-patch.*

| Geometrical parameters | Material constants |
|---|---|
| $\mu=1,\ m=2$ | $E_b=210GPa,\ \eta_b=0.001$ |
| $h_b=0.0025m,\ b=0.02m$ | $\rho_b=7800kg/m^3,\ \rho_p=7500kg/m^3$ |
| $x_0=0.01m,\ h_0=0.0001m$ | $s_{xx}^E=1.65\times10^{-11}m^3/N$ |
| $x_1=0.05m,\ x_2=0.10m$ | $\epsilon_{zz}^T=3.01\times10^{-8}F/m$ |
| $x_{p1}=0.01m,\ x_{p2}=0.05m$ | $d_{xz}=-2.74\times10^{-10}C/m^2$ |
| $x_f=0.075m,\ F=1N$ | $R=100\Omega$ |

### 3.2 Effects of the resistance and its energy dissipation characteristics

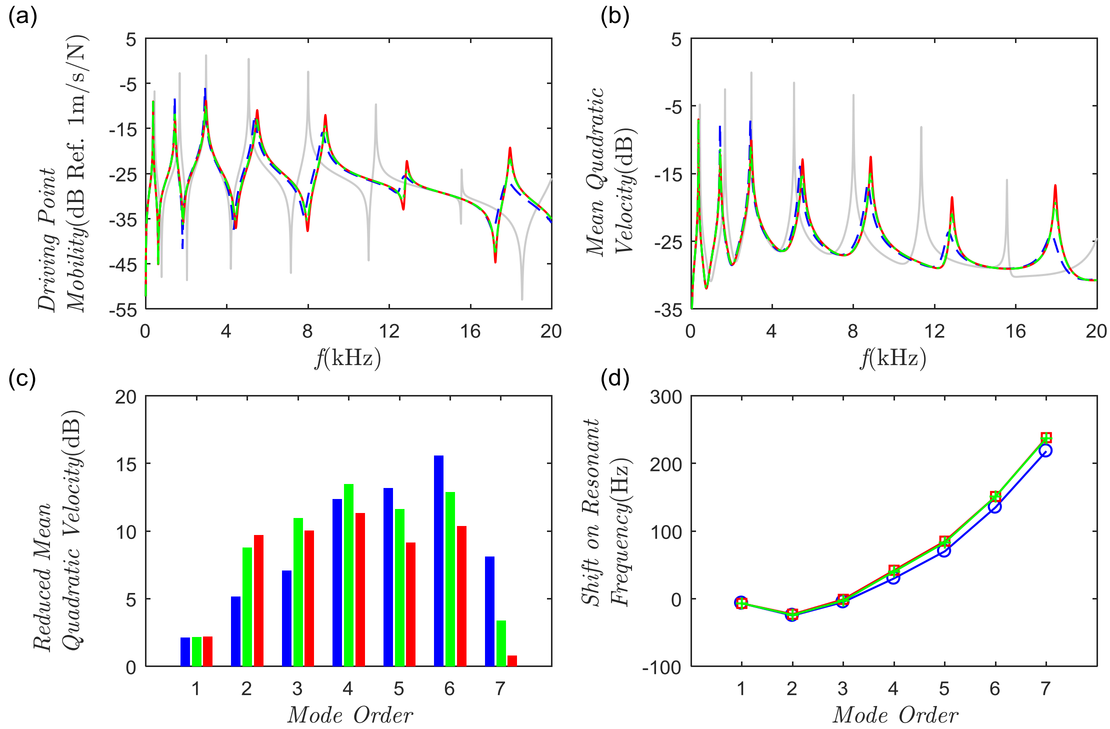


*Fig. 2. Frequency responses of the ABH beam with resistance of the shunting circuit taken by 100Ω (in blue), 500Ω (in green), and 1000Ω (in red): (a) driving point mobility; (b) mean quadratic velocity of the uniform part; (c) mean quadratic velocity reduction at resonant frequencies; (d) shifts on resonant frequencies. The gray lines in (a) and (b) correspond to a bare ABH beam.*

The driving point mobility of the beam is presented in Fig. 2(a) in which the resistance is respectively set as 100Ω, 500Ω, and 1000Ω, together with that of a bare ABH beam. To show the overall vibration level, the mean quadratic velocity of the beam's uniform part (hereafter abbreviated as the mean quadratic velocity) is plotted in Fig. 2(b) for all cases. Substantial vibration reductions are observed in both single-point and overall responses of the beam, which becomes more pronounced at higher frequencies due to the taper's energy concentration effect.

The differences caused by different resistances, however, show a clear frequency dependency. To understand this dependency, we summarize the specific values of the reduced mean quadratic velocity at the first seven resonant frequencies in Fig. 2(c) and shifts of these frequencies compared to those of a bare beam in Fig. 2(d). It can be seen reductions caused by three resistances are equally small at the first resonance — which is understandable since the first mode of the beam is not dominated by its ABH part — and grow at different rates afterwards. The 1000Ω-resistance gains its maximum at the second resonance, 500Ω at the third and the fourth, and 100Ω leads the rest. For the resonant frequencies, on the other hand, all three cases show a similar and positive shift except for the first two.

Such behavior of the beam is resulted, in essence, from the frequency-dependent elasticity modulus of the piezo-patch $E_p$ . The amplitudes of $E_p$ with 100Ω-, 500Ω-, and 1000Ω-resistance are shown in Fig. 3(a). The equivalent loss factor of the patch $\eta_p$, defined as the ratio between $E_p$'s imaginary part and real part, is shown in Fig. 3(b). The energy ratio between the ABH part and the uniform part, *i.e.* $\Gamma = 10\log\langle \dot{w}^2 \rangle_{ABH} / \langle \dot{w}^2 \rangle_{Uni}$, could have been used to measure the influences of $E_p$ and $\eta_p$ on ABH effect. However, as shown in Fig. 3(c), the complexity resulted from the frequency-dependency makes it rather difficult to recognize a clear pattern. We use the reflection coefficient to give a better explanation, which is written as

$$R = e^{2\int_{x_0}^{x_1} \mathrm{Im}k_b(x)dx} \tag{10}$$

where $\mathrm{Im}k(x)$ means the imaginary part of bending wavenumber $k_b(x)$.

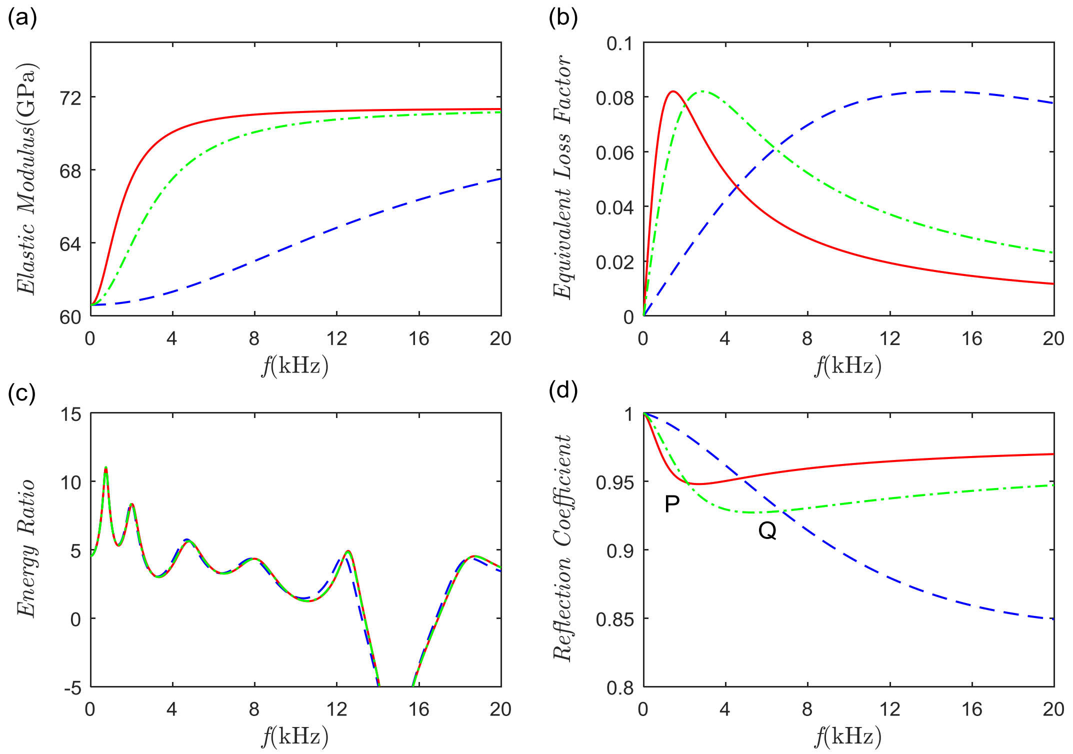


*Fig. 3. Energy dissipation characteristics of the ABH beam when resistance of the shunting circuit takes values of 100Ω (blue dash line), 500Ω (green dotted dash line), and 1000Ω (red solid line): (a) elastic modulus of the piezo-patch; (b) equivalent loss factor of the piezo-patch; (c) energy ratio between the ABH and uniform parts; (d) reflection coefficient of the ABH taper.*

The reflection coefficient gives the extent to which an incoming bending wave is reflected back by the ABH taper, implying a lower coefficient predicts a better ABH effect. Though by no means perfect, the reflection coefficient serves as a simple mean to look into the underlying mechanisms. The reflection coefficient of an ABH beam with a certain resistance is divided into three phases along the frequency axis, separated by *P* and *Q* in Fig. 3(d). Before *P*, both $E_p$ and

$\eta_p$ are small, and the main influence of piezo-patch on the beam is its mass-loading effect, which causes the negative shifts of the first two resonant frequencies. From $P$ to $Q$, the increased energy dissipation resulted from the rise of $\eta_p$ effectively lowers the reflection coefficient, leading to an inverse symmetry between the two curves. After Q, $E_p$ dominates the reflection coefficient. The fast increase of 500Ω-$E_p$ and 1000Ω-$E_p$ largely stiffens the beam, creating an intensified impedance-match that substantially weakens the taper's ability to absorb bending wave. It also contributes to the positive shifts of higher-order resonances. The 100Ω-$E_p$ on the other hand, albeit also growing, its moderate rate and lower final value enables the damping effect brought about by a rising loss factor not to be completely offset, leading to a much better performance in the final phase as compared with the other two.

## 4. Experimental Validation

Experiments are conducted to verify the reliability of the proposed characterization method, as well as to affirm the enhancements brought about by the piezo-patch. The test sample is fabricated by the 3D printing technique using UV curable resin. Accordingly, the piezo-patches are replaced by piezo-films with much less density and thickness, to avoid an overwhelming mass-loading effect. The beam was excited by an electromagnetic shaker (BK 4810), with the force measured by a transducer (BK 59571). The shaker was fed with a periodic chirp signal (1~10kHz) generated by a Polytec scanning laser vibrometer and amplified by a power amplifier (BK 2706). The vibrometer was also used to scan the beam on 500 points uniformly located along the middle line.

The results given by the proposed method and the experimental measurement are compared in terms of the cross point mobilities $10\log\left[\dot{w}(x_0)/f(x_f)\right]$, as shown in Fig. 14(a). It can be see the two sets of result are in good agreement, especially at lower frequencies. Those higher-frequency errors are caused by, in addition to the neglected shear deformation and rotary inertia, the underestimated structural damping of the beam. The resin's structural damping is much higher than a steel and is frequency-dependent in nature. Using a uniform loss factor to approximate it can be inaccurate. Nevertheless, the overall consistency of the two sets of result has proven the reliability of the proposed method.

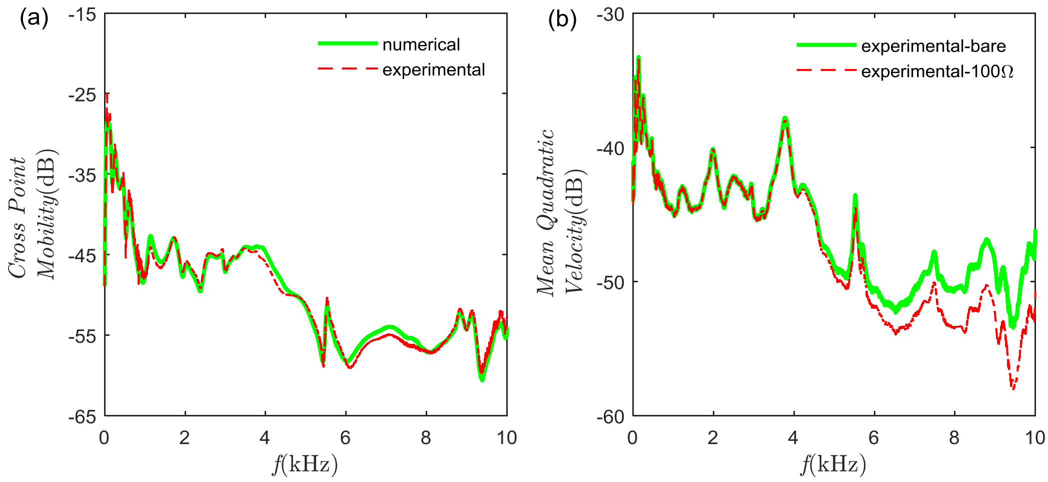


*Fig. 14. Experimental results of the ABH beam with shunted piezo-film: (a) comparison of cross point mobility given by experiment and simulation; (b) comparison of mean quadratic velocity obtained from the ABH beam with and without a shunted piezo-film.*

## 5. CONCLUSIONS

This paper uses the shunted piezo-electric patch to enhance the ABH effect in an Euler-Bernoulli beam, a phenomenon created by a power-law profiled taper insertion and consequently suffers from the unavoidable truncation at the tip. To pave the way for this study, an energy-based numerical model is first built for the patch-beam coupled system. Based on this model, the effects of shunting circuit's resistance on the ABH effect, together with its energy dissipation characteristic, are discussed. Experiments are performed at last to validate both the characterization method and the enhancements brought about by the shunted piezo-electric patch.

## 6. REFERENCES


1. M.A. Mironov, Propagation of a flexural wave in a plate whose thickness decreases smoothly to zero in a finite interval, Soviet Physics: Acoustics 34 (3) (1988) 318-319.
2. V.V. Krylov, A.L. Shuvalov, Propagation of localized flexural vibrations along plate edges described by a power law, Proceedings of the Institute of Acoustics 22 (2) (2000) 263–270.
3. D.J. O'Boy, V.V. Krylov, V. Kralovic, Damping of flexural vibrations in rectangular plates using the acoustic black hole effect, Journal of Sound and Vibration 329 (22) (2010) 4672–4688.
4. V.E. Gusev, C. Ni, A. Lomonosov, Z. Shen, Propagation of flexural waves in inhomogeneous plates exhibiting hysteretic nonlinearity: nonlinear acoustic black holes, Ultrasonics 61 (2015) 126–35.
5. V. Denis, F. Gautier, A. Pelat, J. Poittevin, Measurement and modelling of the reflection coefficient of an acoustic black hole termination, Journal of Sound and Vibration 349 (2015) 67–79.
6. S. Yan, A.M. Lomonosov, Z. Shen, Evaluation of an acoustic black hole's structural characteristics using laser-generated lamb waves, Laser Physics Letter 13 (2) (2016) 025003.